EPJ Web of Conferences **170**, 02008 (2018) https://doi.org/10.1051/epjconf/201817002008
ANIMMA 2017

Radiation induced currents in mineral-insulated cables and in pick-up coils: model calculations and experimental verification in the BR1 reactor

Ludo Vermeeren, Willem Leysen and Benoit Brichard

***Abstract* — Mineral-insulated (MI) cables and Low-Temperature Co-fired Ceramic (LTCC) magnetic pick-up coils are intended to be installed in various position in ITER. The severe ITER nuclear radiation field is expected to lead to induced currents that could perturb diagnostic measurements. In order to assess this problem and to find mitigation strategies models were developed for the calculation of neutron- and gamma-induced currents in MI cables and in LTCC coils.**

The models are based on calculations with the MCNPX code, combined with a dedicated model for the drift of electrons stopped in the insulator. The gamma induced currents can be easily calculated with a single coupled photon-electron MCNPX calculation. The prompt neutron induced currents requires only a single coupled neutron-photon-electron MCNPX run. The various delayed neutron contributions require a careful analysis of all possibly relevant neutron-induced reaction paths and a combination of different types of MCNPX calculations.

The models were applied for a specific twin-core copper MI cable, for one quad-core copper cable and for silver conductor LTCC coils (one with silver ground plates in order to reduce the currents and one without such silver ground plates). Calculations were performed for irradiation conditions (neutron and gamma spectra and fluxes) in relevant positions in ITER and in the Y3 irradiation channel of the BR1 reactor at SCK•CEN, in which an irradiation test of these four test devices was carried out afterwards.

We will present the basic elements of the models and show the results of all relevant partial currents (gamma and neutron induced, prompt and various delayed currents) in BR1-Y3 conditions. Experimental data will be shown and analysed in terms of the respective contributions. The tests were performed at reactor powers of 350 kW and 1 MW, leading to thermal neutron fluxes of 1E11 n/cm²s and 3E11 n/cm²s, respectively. The corresponding total radiation induced currents are ranging from 1 to 7 nA only, putting a challenge on the acquisition system and on the data analysis.

The detailed experimental results will be compared with the corresponding values predicted by the model. The overall agreement between the experimental data and the model predictions is fairly good, with very consistent data for the main delayed current components, while the lower amplitude delayed currents and some of the prompt contributions show some minor discrepancies.

***Index Terms*—ITER, LTCC pick-up coils, Mineral-Insulated Cables, Neutrons, Radiation effects**

I. Introduction

During the burning process in ITER, a large amount of radiation will be released mainly in the form of energetic neutrons and gamma-rays. Due to their uncharged state, neutrons and gamma-rays can easily escape the plasma and potentially damage (either permanently or temporarily) components and devices, such as ITER Diagnostic Components installed in ITER [1,2]. Magnetic Pick-Up Coils and mineral-insulated (MI) cables are intended to be installed in the divertor region and in the ITER vessel behind the blanket modules. The Magnetic Pick-Up Coils are fabricated based on the Low Temperature Co-fired Ceramic (LTCC) technology [3,4]. In view of the high ITER nuclear radiation field at the locations of these items a specific study of radiation effects on MI cables and LTCC coils was performed. In this paper we discuss the radiation induced currents between the inner conductors and the grounded parts of the devices, as these currents might perturb the proper functioning of the devices. Elaborating the approach described in [5] and [6], we will present MCNPX [7] based models for the calculation of the various contributions to the radiation induced currents and we will discuss an irradiation test in the BR1 research reactor at SCK•CEN proving the validity of the models.

II. Description of the Devices Under Test

A. Description of the selected MI cables

One MI cable with two inner copper conductor (twin-core) and one with four inner copper conductors (quad-core) were selected for this study, both with magnesia insulator and with

This work was supported by F4E via the contract F4E-OFC-358-01-01-03.

Ludo Vermeeren and Willem Leysen are with the Belgian Nuclear Research Center, SCK•CEN, Boeretang 200, BE-2400 Mol, Belgium (e-mails: ludo.vermeeren@sckcen.be and willem.leysen@sckcen.be).

Benoit Brichard is with Fusion for Energy, Av. Josep Pla 2, Torres Diagonal Litoral B3, 08019 Barcelona, Spain (e-mail: benoit.brichard@f4e.europa.eu).

AISI 316L sheath (containing approximately resp. 0.81% and 1.64% Mn). The twin-core MI cable has an outer diameter of 4.2 mm and a conductor diameter of 0.8 mm. The quad-core MI cable has an outer diameter of 3.6 mm and a conductor diameter of 0.44 mm. For the model calculations, the cables are considered to be infinitely long and the results are presented per unit length.

B. Description of the LTCC pick-up coils

The LTCC magnetic sensor prototypes consist of a sintered stack of ceramic layers with printed metallic circuits, which constitute a number of conductive turns connected in series in order to obtain a magnetic pick-up coil. Figure 1 illustrates the external layout of the prototypes as well as the inside part showing the wiring.

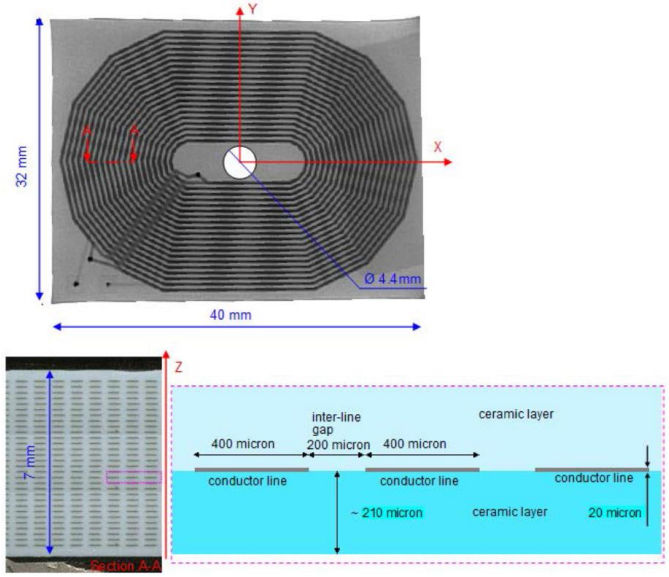

Fig. 1. details on the geometry and the winding pattern of the LTCC sensor prototypes

Two types of LTCC sensors were studied; both of them have silver as conductor material and DuPont-951 ceramic [8] as ceramic insulator. The composition of the latter material was approximated as 43 at% Al + 31 at% Si + 20 at% O + 6 at% Ca, with a density of 3.1 g/cm³. Both LTCC sensors have nominal dimensions of 40mm*32mm*7mm and are composed of a bulk DuPont-951 ceramic part, a 30 layer electrical circuit embedded in the ceramic and two electrical contacts equipped with a pair of copper wires connecting to the measuring equipment. For one of them, 50 µm thick silver ground plates (with 40% effective surface) were added at the lower and upper side of the sensor, each of them connected to a copper wire. The aim of these plates is to counterbalance the neutron induced current in the silver windings, thus reducing the net current.

III. MCNPX MODELLING

A. Basic principles

Neutron and gamma-induced interactions lead to the generation of a current between the inner conductors and the grounded parts [5]. After the impact of neutrons or gammas, several possible interactions lead to the creation of energetic electrons. A fraction of these free electrons is sufficiently energetic to cross the insulator. These electrons constitute a current between the inner conductors and the grounded parts. Conventionally, currents are taken positive if electrons cross the insulator from the core wire towards the ground. If the 'circuit' is closed by connecting a current meter, this corresponds to a positive (conventional) current through the meter from the central conductor side to the ground.

Two classes of free electron generating processes can be considered. On one hand, the production of beta rays upon decay of unstable isotopes formed after neutron capture leads to a delayed current with a response time depending on the half-life of the activation product. On the other hand, prompt processes stem from external gamma rays — or from gamma rays produced quasi-instantaneously after neutron interactions — creating free electrons by photoelectric effect, Compton scattering, or pair formation.

In principle, the following contributions to the induced current can be identified:

A. I(n,β_core): current due to neutron interactions in the central conductor and subsequent beta decay
B. I(n, β_insulator): current due to neutron interactions in the insulator and subsequent beta decay
C. I(n, β_ground): current due to neutron interactions in the (grounded) sheath and subsequent beta decay
D. I(n, β_surrounding): current due to neutron interactions in the sensor surroundings (if applicable) and subsequent beta decay
E. I(n,γ,e): current due to gammas created by neutron interactions in the sensor (and, if applicable, in the surroundings) and subsequent gamma-electron interactions
F. I(γ,e): current due to fast electrons generated in the sensor (and, if applicable, in the surroundings) by external gammas

Components E and F each require one single MCNPX calculation: starting from a neutron or gamma source at the outer surface of the sensor (with the appropriate spectrum), the deposited charge in the relevant parts of the cable is calculated directly, including all (prompt) interactions between neutrons, gammas and electrons.

On the other hand, MCNPX does not include the delayed effects related to beta decay of activation products, so these contributions have to be modelled explicitly. This requires two steps: (1) the reaction rate of each possible contribution should be calculated, and (2) an electron transport calculation should be performed for each contribution, starting from the appropriate beta source (spectrum, and, if relevant, spatial distribution); this second step yields the deposited charges in the relevant parts of the cable per source beta.

For thermal neutrons, neutron capture (the (n,γ) reaction) is the dominant reaction. But for a spectrum with a high contribution of fast neutrons like the ITER spectrum, several other reaction channels can be open, like (n,2n), (n,p) and (n,α). For all these reactions on all isotopes present in the sensor, it should be analyzed whether a beta-emitting nucleus is formed and a preliminary assessment of the possible contribution to the RIEMF current is required based on the atomic concentration of the isotope, on the cross section of the reaction, on the half-life of the activation product and on the beta end-point energy.

For the cable core wires (pure copper), both natural Cu isotopes contribute in principle through the following schemes:

- $^{63}Cu(n,\gamma)^{64}Cu(\beta+ \text{ decay})\text{-->}^{64}Ni$, $T_{1/2} = 12.7$ h (61%)
- $^{63}Cu(n,\gamma)^{64}Cu(\beta- \text{ decay})\text{-->}^{64}Zn$, $T_{1/2} = 12.7$ h (39%)
- $^{63}Cu(n,2n)^{62}Cu(\beta+ \text{ decay})\text{-->}^{64}Zn$, $T_{1/2} = 9.74$ min
- $^{65}Cu(n,\gamma)^{66}Cu(\beta- \text{ decay})\text{-->}^{66}Zn$, $T_{1/2} = 5.12$ min
- $^{65}Cu(n,2n)^{64}Cu(\beta+ \text{ decay})\text{-->}^{64}Ni$, $T_{1/2} = 12.7$ h (61%)
- $^{65}Cu(n,2n)^{64}Cu(\beta- \text{ decay})\text{-->}^{64}Zn$, $T_{1/2} = 12.7$ h (39%)
- $^{65}Cu(n,p)^{65}Ni(\beta- \text{ decay})\text{-->}^{65}Cu$, $T_{1/2} = 2.52$ h

The cable insulators are composed of magnesium and oxygen. After analysis, the retained contributions are:

- $^{24}Mg(n,2n)^{23}Mg(\beta+ \text{ decay})\text{-->}^{23}Na$, $T_{1/2} = 11.3$ s
- $^{24}Mg(n,p)^{24}Na(\beta- \text{ decay})\text{-->}^{24}Mg$, $T_{1/2} = 14.96$ h
- $^{16}O(n,2n)^{15}O(\beta+ \text{ decay})\text{-->}^{15}N$, $T_{1/2} = 2.03$ min
- $^{16}O(n,p)^{16}N(\beta- \text{ decay})\text{-->}^{16}O$, $T_{1/2} = 7.13$ s

The cable sheaths contain mainly iron, nickel and chromium, and also about 1.5% of manganese. The relevant reactions are:

- $^{56}Fe(n,p)^{56}Mn(\beta- \text{ decay})\text{-->}^{56}Fe$, $T_{1/2} = 2.58$ h
- $^{58}Ni(n,p)^{58}Co(\beta+ \text{ decay})\text{-->}^{58}Fe$, $T_{1/2} = 70.8$ d
- $^{60}Ni(n,p)^{60}Co(\beta- \text{ decay})\text{-->}^{60}Ni$, $T_{1/2} = 5.272$ a
- $^{64}Ni(n,\gamma)^{65}Ni(\beta- \text{ decay})\text{-->}^{65}Cu$, $T_{1/2} = 2.52$ h
- $^{52}Cr(n,p)^{52}V(\beta- \text{ decay})\text{-->}^{52}Cr$, $T_{1/2} = 3.75$ min
- $^{55}Mn(n,\gamma)^{56}Mn(\beta- \text{ decay})\text{-->}^{56}Fe$, $T_{1/2} = 2.58$ h

For the LTCC windings (pure silver), both natural Ag isotopes contribute in principle through the following schemes:

- $^{107}Ag(n,\gamma)^{108}Ag(\beta- \text{ decay})\text{-->}^{108}Cd$, $T_{1/2} = 2.41$ min
- $^{107}Ag(n,2n)^{106}Ag(\beta+ \text{ decay})\text{-->}^{106}Pd$, $T_{1/2} = 24$ min
- $^{109}Ag(n,\gamma)^{110}Ag(\beta- \text{ decay})\text{-->}^{110}Cd$, $T_{1/2} = 24.6$ s
- $^{109}Ag(n,2n)^{108}Ag(\beta- \text{ decay})\text{-->}^{108}Cd$, $T_{1/2} = 2.41$ min
- $^{109}Ag(n,p)^{109}Pd(\beta- \text{ decay})\text{-->}^{109}Ag$, $T_{1/2} = 13.43$ h

All these contributions are taken into account in the calculations. In principle, also the metastable states ^{106m}Ag, ^{108m}Ag and ^{110m}Ag are populated by the mentioned reactions, but these are neglected here, since:

(1) ^{106m}Ag decays via electron capture only, emitting no betas;

(2) ^{108m}Ag decays via internal transitions and electron capture, emitting no betas (moreover, it has a half-life of 418 years, so the decay rate is very low);

(3) ^{110m}Ag has three main decay paths: 2% via internal transitions (no beta), 67% via beta decay with a beta end-point energy of 0.06 MeV only (so all emitted betas will be stopped locally) and 31% via beta decay with a beta end-point energy of 0.51 MeV only (so an average beta energy of about 0.2 MeV, which is also not sufficient to contribute efficiently to the current; moreover, the half-life is long (250 days), leading anyway to low decay rates.

The mentioned schemes also apply to the contributions from the grounded silver planes (if present), but, as in that case the betas originate from the other electrode, the sign is inverted.

The LTCC insulator material is supposed to be composed of aluminum, silicon, oxygen and a small fraction of calcium. After analysis, the retained contributions are:

- $^{27}Al(n,\gamma)^{28}Al(\beta- \text{ decay})\text{-->}^{28}Si$, $T_{1/2} = 2.25$ min
- $^{27}Al(n,p)^{27}Mg(\beta- \text{ decay})\text{-->}^{27}Al$, $T_{1/2} = 9.46$ min
- $^{27}Al(n,\alpha)^{24}Na(\beta- \text{ decay})\text{-->}^{24}Mg$, $T_{1/2} = 14.96$ h
- $^{28}Si(n,p)^{28}Al(\beta- \text{ decay})\text{-->}^{28}Si$, $T_{1/2} = 2.25$ min
- $^{30}Si(n,\gamma)^{31}Si(\beta- \text{ decay})\text{-->}^{31}P$, $T_{1/2} = 2.62$ h
- $^{16}O(n,p)^{16}N(\beta- \text{ decay})\text{-->}^{16}O$, $T_{1/2} = 7.13$ s

B. Special treatment of electrons stopped in the insulator

MCNPX only calculates the particle transport down to a pre-set lower energy limit. More specifically, the electron transport is calculated until an energy of 1 keV at which it is supposed to remain at the same position. The subsequent drift of electrons out of the insulator under the action of the created space charge field is not calculated by MCNPX. Part of these electrons will drift back to the beta emitting cell, and another part to the other electrode; only the latter electrons will contribute to the current. So the calculation of the current requires an extra calculation step. For cylindrically symmetric configurations, formalisms have been developed to determine the fraction f of electrons drifting back to the original electrode, e.g. [9].

For the geometries considered here, the cylindrical symmetry is broken, so the simple analytical model cannot be applied anymore. Therefore, a similar procedure as in [5]. was followed: the Poisson equation was solved in an iterative way, assuming a constant charge density and zero boundary conditions. From the resulting space charge field profile, the zero-field surface was deduced and introduced as an additional surface in MCNPX to subdivide the insulator in two parts: a part close to the copper wires (in which all the deposited betas are supposed to drift towards the copper wires) and a part close to the sheath (in which all deposited betas are supposed to drift towards the sheath).

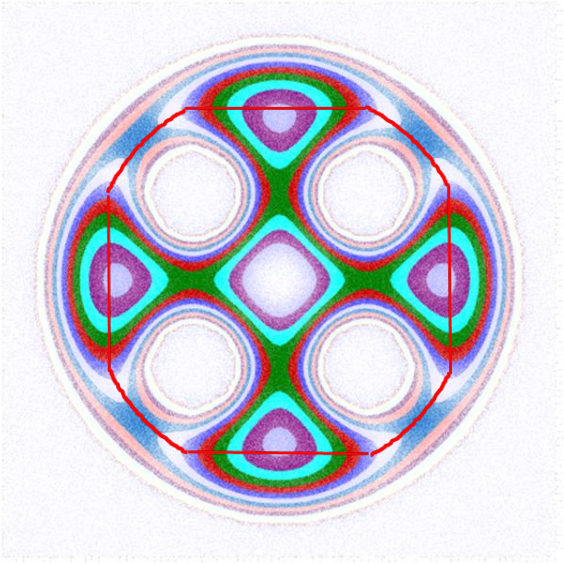

Fig. 2. Calculated space charge potential profile for the quad-core MI cable, with the deduced zero-field surface shown as a red line

To determine the boundary surface for the cables, a rectangular 2D grid is defined representing the insulator and the Poisson equation for the space charge potential is solved, assuming a homogeneous charge deposition and zero potential boundaries at the interfaces with the core wires and the sheath. This is done in Excel by iteratively calculating each cell as the average of the potentials in each of the four neighbours plus a constant value (the space charge density, which for our purpose can take any non-zero value). As an example, the resulting potential contours for the quad-core cable are shown in Figure

2, together with the deduced zero-field surface approximation: a combination of four symmetric planes defined by x,y=±0.94mm and a concentric cylinder with radius 1.1 mm.

For the planar LTCC geometry, the zero field surfaces are assumed to be in the middle of the insulator parts.

C. Calculation of prompt neutron induced contribution

A coupled neutron-photon-electron MCNPX calculation is performed, starting from a neutron source which is uniformly distributed at the outer surface of the cable (or at a cylindrical surface enveloping the LTCC), with an inward initial direction distribution proportional to the cosine of the angle with the normal to the surface, and with the relevant energy spectrum. As output we obtain the deposited charge in each cell of the geometry. MCNPX provides the results normalized per source particle. In order to normalize the results to the neutron flux, the neutron flux per source neutron is calculated by MCNPX too.

The effective charge transfer per source neutron from the central conductor to the grounded parts can be calculated as the total charge deposited in the central conductors and in the surrounding insulator parts.

The total prompt neutron induced current (for the cables per unit length) can then be calculated by dividing the effective charge transfer per source neutron by the ratio between the real flux and the flux per source neutron.

D. Calculation of prompt gamma induced contribution

This calculation follows the same procedure as for the prompt neutron contribution, only a suitable gamma source is defined instead of a neutron source and a couples photon-electron MCNPX calculation is performed.

E. Calculation of delayed neutron induced contributions

First, for each geometry and each neutron spectrum of interest, a "neutron only" MCNPX calculation is performed in order to obtain the rate densities of all reactions specified in Section III.A. The JEFF-3.2 neutron cross section library [10] was consistently used for all calculations.

Each of the considered reactions leads to the formation of a beta-emitting isotope (with a certain half-life); so, in equilibrium conditions, each reaction corresponds to one decay. The decay properties (involving beta emission) were studied in detail for each isotope involved: the relative probabilities of beta-plus decay paths (with possibly various beta end point energies), of beta-minus decay paths (with possibly various beta end point energies), and of decay paths without beta emission (mainly electron capture). The beta spectra were calculated as the sum of the corresponding Fermi beta distribution functions.

In order to obtain the induced current, one needs to calculate the probability that an emitted beta effectively contributes to the current, i.e. the probability that it crosses the insulator. This calculation is done by an "electron only" MCNPX calculation. After defining the problem geometry in MCNPX, an electron source is defined with the appropriate beta spectral distribution and homogeneously distributed within the appropriate cells (and with random initial direction). As output from MCNPX we obtain the charge deposition in each cell (normalized per source electron). The effective charge transfer per source electron from central conductors to ground can be calculated as the total charge deposited in the central conductors and in the surrounding insulator parts.

Each (equilibrium) delayed neutron-induced current contribution is then calculated as the product of the MCNPX reaction rate density, the volume of the cell in which the interactions take place, the effective charge transfer per beta (with the correct sign, depending on whether positrons or electrons are the charge carriers), the number of betas per decay, and the ratio between the real flux and the flux (per source neutron per second) as outputted by MCNPX.

IV. MCNP RESULTS

A. Neutron and gamma spectra

Calculations were performed for typical ITER conditions, as well as for the conditions in the Y3 channel of the BR1 reactor at SCK•CEN, in which validation tests were performed later on. Figs. 3 and 4 show the BR1 neutron and gamma spectral data used for the calculations (total neutron flux 5.998 10^{11} n/(cm²s), total gamma flux 7.9 10^{10} γ/(cm²s)). The total neutron and gamma fluxes at the location of the MI cables in ITER was assumed to be 2.28 10^{13} n/(cm²s) and 2.1 10^{13} γ/(cm²s)); the fluxes at the LTCC coil location were taken as 1.41 10^{13} n/(cm²s) and 0.72 10^{13} γ/(cm²s)).

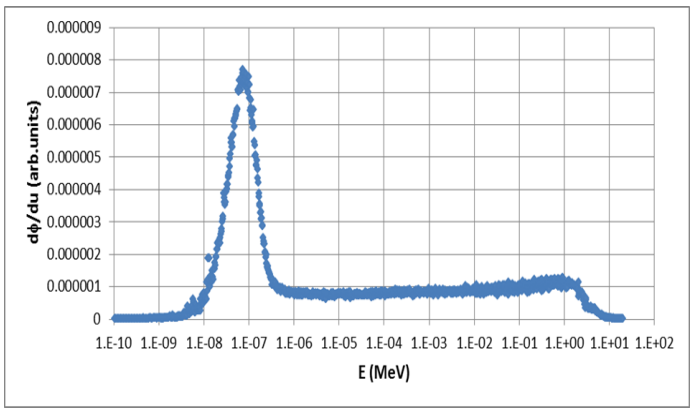

Fig. 3. Neutron spectrum used as input for the BR1 calculations

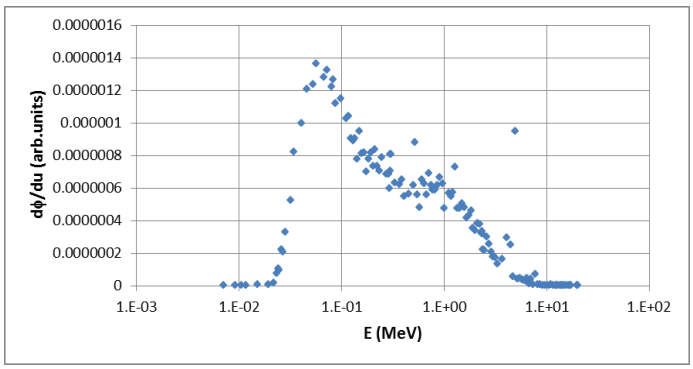

Fig. 4. Gamma spectrum used as input for the BR1 calculations

B. MI cables

Table I shows the calculated absolute current contributions of the various processes in the twin-core and the quad-core MI cable (in nA per m cable length, sum of all wires) for the BR1 case. Similar calculations were performed for the ITER case.

TABLE I

Process	2-core	4-core
$^{63}Cu(n,\gamma)^{64}Cu$	0.0015 nA	0.017 nA
$^{65}Cu(n,\gamma)^{66}Cu$	0.54 nA	0.44 nA
$^{64}Ni(n,\gamma)^{65}Ni$	-0.001 nA	-0.001 nA
$^{55}Mn(n,\gamma)^{56}Mn$	-0.132 nA	-0.223 nA
Prompt neutron	0.78 nA	0.47 nA
Prompt gamma	0.05 nA	0.08 nA
Total	1.12 nA	0.80 nA

The prompt neutron contribution appears to be dominant. Amongst the delayed contributions, the $^{65}Cu(n,\gamma)^{66}Cu$ reaction is the dominant reaction, leading to a main response time of 5.1 min / (ln(2)) = 7.36 min. The contribution by the $^{55}Mn(n,\gamma)^{56}Mn$ reaction is also rather large and negative; its response time is much larger: 2.58 h / ln(2)) = 4.04 h. The results for the ITER case show non-negligible contributions from the $^{63}Cu(n,2n)^{62}Cu$ reaction (response time 9.74 min / ln(2)) = 14.05 min) and the $^{16}O(n,p)^{16}N$ reaction (response time 7.13 s / ln(2)) = 10.5 s); the prompt gamma contribution is also very important in that case.

C. LTCC coils

Table II summarizes the calculated absolute current contributions of the various processes for the LTCC coils without ground plate and with silver ground plates (20µm effective thickness) in the BR1 conditions. Similar calculations were performed for the ITER case.

TABLE II

Process	No ground plate	With ground plate
from windings		
$^{107}Ag(n,\gamma)^{108}Ag$	0.5 nA	0.5 nA
$^{109}Ag(n,\gamma)^{110}Ag$	3.6 nA	3.2 nA
from ground plate		
$^{107}Ag(n,\gamma)^{108}Ag$	-	-0.44 nA
$^{109}Ag(n,\gamma)^{110}Ag$	-	-1.9 nA
from insulator		
$^{27}Al(n,\gamma)^{28}Al$	0.4 nA	0.2 nA
$^{30}Si(n,\gamma)^{31}Si$	0.003 nA	0.001 nA
Prompt neutron	2.0 nA	2.0 nA
Prompt gamma	0.2 nA	0.2 nA
Total	6.7 nA	3.8 nA

In the BR1 case, the dominant contributions are the prompt neutron current and the current due to beta decay of ^{110}Ag, formed after neutron capture by ^{109}Ag. In the ITER case, the gamma induced current becomes dominant and additional delayed components due to (n,p), (n,α) and (n,2n) reactions are also contributing to some extent.

When adding two silver ground plates (each with effective thickness 20 µm), an extra current with opposite sign is generated, due to activation and decay of silver nuclei in these ground plates. The resulting total current is about a factor 2 lower than in the geometry without ground plates.

V. Experimental test in the BR1 reactor

The MIC and LTCC coils were irradiated in the Y3 channel of the BR1 reactor. BR1 is an air cooled graphite moderated thermal reactor with a nominal thermal power of 700 kW; for short periods the power can be raised to 1 MW. The thermal and epithermal neutron flux at the center of channel Y3 were determined by activation dosimetry, using an Al/Co and an Al/Ag foil, placed near the LTCC coils. For the reference BR1 power of 700 kW, the conventional thermal neutron flux was found to be 1.98 10^{11} n/(cm²s) and the epithermal flux per unit lethargy 1.5 10^{10} n/(cm²s). Taking into account the neutron spectrum used for the calculations, the measured thermal neutron flux corresponds to a total neutron flux of 4.5 10^{11} n/(cm²s).

For the LTCC coil calculations, a reference total flux of 5.998 10^{11} n/(cm²s) was assumed; so the model results have to be normalized by a factor 4.5/5.998 to get the results for the real conditions at 700 kW.

The ends of the MI cables were also positioned near the center of the Y3 channel, but they extend over half of the reactor axis, through the reflector and the shielding to the side of the reactor. In order to obtain the integrated flux over the complete cable length, the known axial neutron flux profile was used. For a maximum total neutron flux of 4.5 10^{11} n/(cm²s), it leads to a length-integrated total flux of 8.62 10^{11} n/(cm²s)m. Hence, the MCNP model results from should be renormalized by a factor 8.62/5.998 before comparison with the experimental data at 700 kW.

Several test runs at varying conditions were performed with continuous monitoring of the currents and the reactor power. For the first two test runs, the reactor power was ramped up to 350 kW and scrammed after about 30 minutes. In the first case, the currents of the MI cables were measured individually for each core wire, while in the second, all cores wires of each cable were physically connected and the global currents were measured. Similarly two more test runs were performed with the reactor power rising to 350 kW, after 5 minutes stabilization followed by an increase up to 1000 kW, stabilization for 60 minutes, power reduction to 350 kW and scram. The decay of the signals was monitored continuously for about 16 hours.

All recorded MI cable currents were fitted with a least squares procedure as the sum of a constant offset, a prompt signal (proportional to the reactor power), a delayed component due to activation of ^{65}Cu and subsequent decay of ^{66}Cu and a delayed component due to activation of ^{55}Mn (four free parameters). Similarly the LTCC coil current were analyzed as the sum of an offset, a prompt signa and delayed components due to activation of ^{107}Ag and ^{109}Ag.

Figure 5 shows an example of the data recorded for an MI cable: the current from one of the quad-core cable wires during the 1000 kW test run. The fitted partial contributions are included in the graph as well as a plot of the pointwise differences between the total fit curve values and the

experimental data. Taking into account the limited number of free parameters (4) and the uncertainty on the experimental data (including the reactor power data) the agreement is very satisfactory.

Figure 6 shows similar data for the LTCC coil without ground plates and figure 7 for the LTCC coil with ground planes. For the latter, an insulation resistance problem resulted in a strong, slowly varying background. Hence the fitting procedure could not be applied as such; the data could only be analyzed in first order as the sum of a linearly varying background and a total neutron induced component (considered to be prompt).

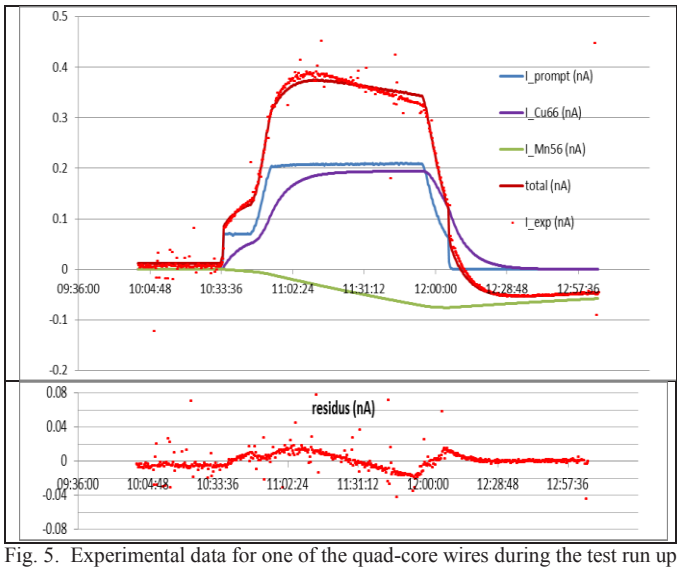

Fig. 5. Experimental data for one of the quad-core wires during the test run up to 1000 kW, including the curves with the various signal contributions, resulting from the fitting procedure; residue plot.

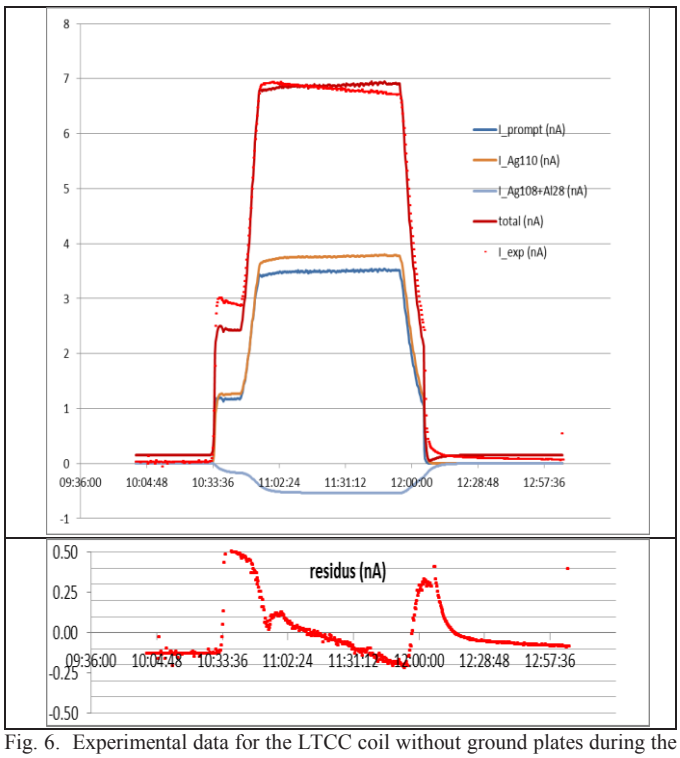

Fig. 6. Experimental data for the LTCC coil without ground plates during the test run up to 1000 kW, including the curves with the various signal contributions, resulting from the fitting procedure; residue plot.

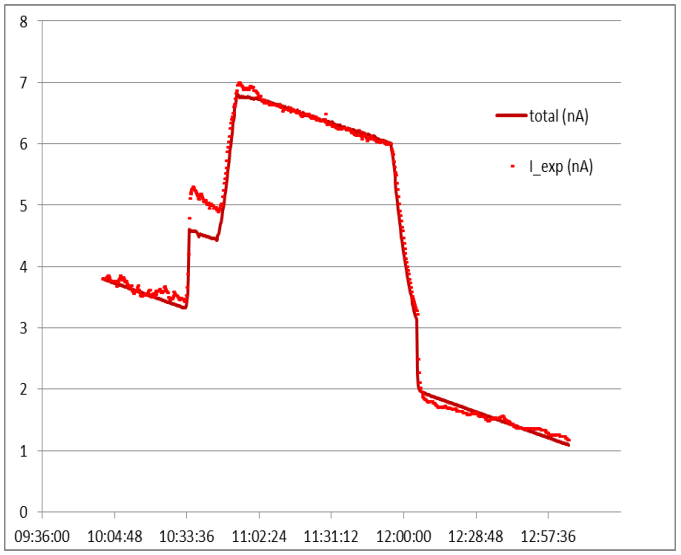

Fig. 7. Experimental data for the LTCC coil with ground plates during the test run up to 1000 kW, including the result of a manual fit assuming a linearly decreasing background.

VI. Validation of the MCNPX based models

Tables III to V summarize the fit results for both MI cables and both LTCCs from an overall analysis and from the analyses of the four runs separately (always normalized to a reactor power of 700 kW). The averages and the standard deviations over the five data sets are also given and the corresponding predicted current contributions from the model are included.

For the twin-core MI cable, the observed prompt current amounts to 55% of the predicted current. Part of this discrepancy can be ascribed to uncertainties in the geometry, the composition of the materials and the neutron/gamma spectra, and also to the fact that surrounding materials in the irradiation setup are not taken into account in the model. However, it is also known [5,11] that especially prompt gamma-induced currents are difficult to model accurately and that significant uncertainties are associated with these particular model results. The observed current contribution due to ^{66}Cu agrees with the model result within about two standard deviations (13% difference) which is considered to be acceptable taken into account all uncertainties. The uncertainty on the observed current contribution due to ^{56}Mn is larger, but it is perfectly consistent with the model prediction (within one standard deviation).

For the quad-core MI cable, the observed prompt current differs from the predicted current by only 30%, which is considered good in view of the modelling uncertainties. The observed current contribution due to ^{66}Cu agrees perfectly with the theoretical result. The experimental current contribution due to ^{56}Mn is larger than the model prediction - possibly since the real MI cable sheath thickness seems to be somewhat larger than the nominal value used for the modelling; still the data agree within 1.5 standard deviations.

TABLE III: ANALYSIS OF TWIN-CORE CABLE DATA

I(nA) @ 700 kW	prompt	^{66}Cu	^{56}Mn
350 kW – A*	0.643	0.938	-0.017
350 kW – B**	0.612	0.972	-0.441
1000 kW – A*	0.664	0.852	-0.275
1000 kW – B**	0.640	0.841	-0.233
overall	0.639	0.863	-0.258
Average+std.dev.	0.64±0.02	0.89±0.05	-0.24±0.14
model	1.17	0.77	-0.19

* sum of the current recorded for the individual wires
** current recorded with joined core wires

TABLE IV: ANALYSIS OF QUAD-CORE CABLE DATA

I(nA) @ 700 kW	prompt	^{66}Cu	^{56}Mn
350 kW – A*	0.502	0.731	-0.261
350 kW – B**	0.466	0.730	-0.560
1000 kW – A*	0.581	0.528	-0.749
1000 kW – B**	0.552	0.464	-0.715
overall	0.531	0.537	-0.767
Average+std.dev.	0.53±0.04	0.60±0.11	-0.61±0.19
model	0.76	0.63	-0.32

* sum of the current recorded for the individual wires
** current recorded with joined core wires

TABLE V: ANALYSIS OF LTCC COIL DATA

I(nA) @ 700 kW	Prompt*	^{110}Ag*	^{108}Ag*	total**
350 kW – A	2.60	2.41	0.223	2.80
350 kW – B	1.99	3.06	0.134	2.94
1000 kW – A	2.41	2.59	-0.367	2.70
1000 kW – B	1.19	3.28	0.005	2.80
overall	1.52	3.31	-0.233	2.59
Average	1.94	2.93	-0.05	2.77
+ std.dev.	±0.53	±0.36	±0.22	±0.12
model	1.71	2.71	0.38	2.80

* LTCC coil without ground plates
** LTCC coil with ground plates

The LTCC coil without any silver ground planes shows a prompt current contribution in very good agreement with the calculation result. The ^{110}Ag related component is also perfectly predicted by the model. The experimental determination of the lower amplitude ^{108}Ag related component was hampered by the quality of the data; moreover, interference with a contribution from activation and decay of aluminum in the supporting structure (leading to a component with a very similar half-life) cannot be excluded. The experimental data give essentially a zero current with a significant uncertainty, while the model predicts a pure ^{108}Ag contribution with an amplitude of almost two times the standard deviation of the experimental results.

Finally, for LTCC7 only a reliable value for the total current could be deduced from the experimental data (due to the significant and varying background). The total expected current of +2.8 nA at a BR1 power of 700 kW is in perfect agreement with the experimental value. Extrapolating the model calculations, a nearly perfect annihilation of the total current could be obtained when using two silver ground plates with an effective average thickness of 50 µm.

So the overall agreement between the experimental data and the MCNPX based model predictions is fairly good, with very consistent data for the main delayed current components, and some minor discrepancies for the lower amplitude delayed currents and some of the prompt contributions.

ACKNOWLEDGMENT

The work leading to this publication has been funded by Fusion for Energy under the Specific Contract F4E-OFC-358-01-01-03. This publication reflects the views only of the authors, and Fusion for Energy cannot be held responsible for any use which may be made of the information contained therein.

REFERENCES

[1] G. Vayakis, E.H. Hodgson, V. Voitsenya and C.I. Walker, Fusion Science and Technology, vol. 55, pp. 699-750, 2008.
[2] G. Vayakis et al., Journal of Nuclear Materials, vol. 417, pp. 780-786, 2011.
[3] G. Chitarin, R. Delogu, A. Gallo and S. Peruzzo, Fusion Engineering and Design, vol. 84, p. 593-598, 2009.
[4] Y. Imanaka, Multilayered low temperature co-fired ceramics (LTCC) technology, Springer, USA, 2005.
[5] L. Vermeeren and R. Van Nieuwenhove, Review of Scientific Instruments 75, pp. 4667-4674, 2003.
[6] S. Peruzzo et al., Fusion Engineering and Design, vol. 88, pp. 1302-1305, 2013.
[7] D.B. Pelowitz, Ed., "MCNPX Users Manual Version 2.7.0" LA-CP-11-00438 (2011).
[8] DuPontTM Green TapeTM 951 Low Temperature Ceramic System, http://www.dupont.com/content/dam/dupont/products-and-services/electronic-and-electrical-materials/documents/prodlib/951.pdf, accessed on May 18, 2017.
[9] N.P. Goldstein, IEEE Transactions on Nuclear Science, vol. NS-20, pp.549-556, 1973.
[10] JEFF-3.2 evaluated data library - Neutron data, https://www.oecd-nea.org/dbforms/data/eva/evatapes/jeff_32/, accessed on May 17,/2017
[11] L. Vermeeren and M. Wéber, Fusion Engineering and Design, vol. 82, pp. 1185-1191, 2007.